

sheet. The maximum value of 90 mA m^{-2} is a lower limit, because we do not resolve the current sheet.

This is, to our knowledge, the first direct evidence of an electric current sheet in the upper solar atmosphere, whose presence has long been predicted. Currents are usually deduced from photospheric vector magnetograms¹⁴. Outside sunspots the interpretation of the photospheric currents is not straightforward, because there the field is highly filamented and unresolved. In the upper chromosphere it has expanded to fill all of space, so that an interpretation in terms of a current sheet is reasonable. Current sheets are thought to be formed spontaneously when the footprints of the Sun's magnetic field are shuffled around^{3,4,15} or when new magnetic flux emerges into the solar atmosphere. Our observations demonstrate that vector spectropolarimetry of the He I 1083.0 nm line allows such current sheets to be detected, thus providing the possibility of observationally testing their importance for the triggering of flares or for coronal heating¹⁶. The presence of such a clear signature in the very first magnetic vector map made with the He I line provides strong support for coronal heating theories based on magnetic energy dissipation at current sheets. □

Received 21 March; accepted 2 September 2003; doi:10.1038/nature02035.

1. Yokoyama, T. & Shibata, K. Magnetic reconnection as the origin of X-ray jets and H-alpha surges in the Sun. *Nature* **375**, 42–44 (1995).
2. Lites, B. W., Skumaniah, A. & Martinez Pillet, V. Vector magnetic fields of emerging solar flux. I. Properties at the site of emergence. *Astron. Astrophys.* **333**, 1053–1068 (1998).
3. Parker, E. N. Magnetic neutral sheets in evolving fields—Part One—General theory. *Astrophys. J.* **264**, 635–641 (1983).
4. Parker, E. N. Magnetic neutral sheets in evolving fields—Part Two—Formation of the solar corona. *Astrophys. J.* **264**, 642–647 (1983).
5. Parker, E. N. Nanoflares and the solar X-ray corona. *Astrophys. J.* **330**, 474–479 (1988).
6. Ulmschneider, P., Priest, E. R. & Rosner, R. (eds) *Mechanism of Chromospheric and Coronal Heating* Ch. 4 (Springer, Berlin/Heidelberg/New York, 1991).
7. Martínez Pillet, V. et al. in *ASP Conf. Ser. 183. High Resolution Solar Physics: Theory, Observation, and Techniques* 264 (Astronomical Society of the Pacific, San Francisco, California, 1999).
8. Harvey, J. & Hall, D. in *IAU Symp. 43. Solar Magnetic Fields* (ed. Howard, R.) 279–288 (Dordrecht, Reidel, 1971).
9. Penn, M. J. & Kuhn, J. R. Imaging spectropolarimetry of the He I 1083 nanometer line in a flaring solar active region. *Astrophys. J.* **441**, L51–L54 (1995).
10. Rüedi, L., Solanki, S. K. & Livingston, W. C. Infrared lines as probes of solar magnetic features. X. He I 10830 Å as a diagnostic of chromospheric magnetic fields. *Astron. Astrophys.* **293**, 252–262 (1995).
11. Rüedi, L., Keller, C. U. & Solanki, S. K. Measurements of the full Stokes vector of He I 10830 Å. *Sol. Phys.* **164**, 265–275 (1996).
12. Handy, B. N. et al. The transition region and coronal explorer. *Sol. Phys.* **187**, 229–260 (1999).
13. Schmidt, W., Muglach, K. & Knölker, M. Free-fall downflow observed in He I 1083.0 nm and Hβ. *Astrophys. J.* **544**, 567–571 (2000).
14. Zirin, H. & Wang, H. Narrow lanes of transverse magnetic field in sunspots. *Nature* **363**, 426–428 (1993).
15. Galsgaard, K. & Longbottom, A. W. Formation of solar prominences by flux convergence. *Astrophys. J.* **510**, 444–459 (1999).
16. Gudiksen, B. V. & Nordlund, Å. Bulk heating and slender magnetic loops in the solar corona. *Astrophys. J.* **572**, L113–L116 (2002).
17. Ruiz Cobo, B. & del Toro Iniesta, J. C. Inversion of Stokes profiles. *Astrophys. J.* **398**, 375–385 (1992).
18. Frutiger, C., Solanki, S. K., Fligge, M. & Bruls, J. H. M. J. Properties of the solar granulation obtained from the inversion of low spatial resolution spectra. *Astron. Astrophys.* **358**, 1109–1121 (2000).
19. Kurucz, R. L. 'Finding' the 'Missing' solar ultraviolet opacity. *Rev. Mexicana Astron. Astrofis.* **23**, 181–186 (1992).
20. Avrett, E. H., Fontenla, J. M. & Loeser, R. in *IAU Symp. 154. Infrared Solar Physics* (ed. Rabin, D. M.) 35–47 (Kluwer Academic, Dordrecht, 1994).
21. Giovanelli, R. G. & Hall, D. The helium 10830 Å line in the undisturbed chromosphere. *Sol. Phys.* **52**, 211–228 (1977).
22. Rachkowsky, D. N. The reduction for anomalous dispersion in the theory of the absorption line formation in a magnetic field [in Russian]. *Izv. Krym. Astrofiz. Obs.* **37**, 56–61 (1967).
23. Trujillo Bueno, J., Landi Degl'Innocenti, E., Collados, M., Merenda, L. & Manso Sainz, R. Selective absorption processes as the origin of puzzling spectral line polarization from the Sun. *Nature* **415**, 403–406 (2002).
24. Lagg, A., Woch, J., Krupp, N. & Solanki, S. K. Retrieval of the full magnetic vector with the He I multiplet at 1083 nm. *Astron. Astrophys.* (submitted).

Acknowledgements M.C. acknowledges support from the Spanish Ministerio de Ciencia y Tecnología. We thank the Kiepenheuer Institut in Freiburg, Germany, for observing support.

Competing interests statement The authors declare that they have no competing financial interests.

Correspondence and requests for materials should be addressed to S.K.S. (solanki@limpi.mpg.de).

The speed of information in a 'fast-light' optical medium

Michael D. Stenner¹, Daniel J. Gauthier¹ & Mark A. Neifeld²

¹Duke University, Department of Physics, and The Fitzpatrick Center for Photonics and Communication Systems, Durham, North Carolina 27708, USA

²Department of Electrical and Computer Engineering, The Optical Sciences Center, University of Arizona, Tucson, Arizona 85721, USA

One consequence of the special theory of relativity is that no signal can cause an effect outside the source light cone, the space-time surface on which light rays emanate from the source¹. Violation of this principle of relativistic causality leads to paradoxes, such as that of an effect preceding its cause². Recent experiments on optical pulse propagation in so-called 'fast-light' media—which are characterized by a wave group velocity v_g exceeding the vacuum speed of light c or taking on negative values³—have led to renewed debate about the definition of the information velocity v_i . One view is that $v_i = v_g$ (ref. 4), which would violate causality, while another is that $v_i = c$ in all situations⁵, which would preserve causality. Here we find that the time to detect information propagating through a fast-light medium is slightly longer than the time required to detect the same information travelling through a vacuum, even though v_g in the medium vastly exceeds c . Our observations are therefore consistent with relativistic causality and help to resolve the controversies surrounding superluminal pulse propagation.

The speed of a light pulse travelling through an optical material is not precisely defined, because any pulse comprises a collection of elementary sinusoidal waveforms, each with a distinct frequency ω . Each constituent sinusoid travels at a well-defined velocity known as the phase velocity $v_p = c/n(\omega)$, where $n(\omega)$ is the refractive index of the optical material. Approximate theories of optical pulse propagation predict that the peak travels at the group velocity $v_g = c/(n + \omega dn/d\omega|_{\omega=\omega_0}) = c/n_g$, where n_g is the group index and ω_0 is the central frequency of the wavepacket⁶.

We refer to the quantity $dn/d\omega$ as the dispersion of an optical material. For typical optical materials, there exist narrow spectral regions where $n(\omega)$ is a decreasing function of frequency (that is, $dn/d\omega < 0$), resulting in a condition known as anomalous dispersion⁷. When ω_0 is within such a region, n_g can be less than one and can even become negative when the anomalous dispersion is large. This results in 'fast light', for which it is possible that the peak of a light pulse may exit the optical material before it passes through the entrance face⁸. The amount of fast-light pulse advancement is largest when v_g is negative and near zero (n_g large and negative).

The possibility of superluminal group velocities ($v_g > c$ or $v_g < 0$) was such a concern to researchers around 1910 that several conference sessions were devoted to the topic⁹. Based on these discussions, Sommerfeld demonstrated theoretically that the velocity of the front of a square-shaped pulse propagating through any medium is identically equal to c and hence relativistic causality is preserved¹⁰. In a follow-up study, Brillouin suggested that the group velocity is not physically meaningful when the dispersion is anomalous because the pulse becomes severely distorted¹¹. More recent research investigating the propagation of smooth-shaped pulses has shown that this conclusion is not justified, leading to renewed controversy^{8,12–20}.

Another outcome of the discussions in the early 1900s, as recounted in the preface and first chapter of the book by Brillouin⁹, was a reformulation of the fundamental postulate of the special theory of relativity. This reformulation states that, rather than limiting the speed of an 'object', it is the information velocity v_i that is limited by c . Unfortunately, there is no agreed-upon definition of the information velocity².

In our experiment, we use a fast-light medium that exploits the spectral region of anomalous dispersion between two closely spaced amplifying resonances^{15,20} realized by creating large atomic coherence²¹ in a laser-driven potassium vapour²², as shown in Fig. 1a. We obtain larger pulse advancement for a smooth gaussian-shaped pulse, as shown in Fig. 1b, in comparison to the experiment of ref. 15, by increasing the gain and hence the size of the anomalous dispersion. The larger advancement relative to the pulse width obtained in our experiment makes it easier to distinguish the different velocities describing pulse propagation. From this data, we infer that $n_g = -19.6 \pm 0.8$, indicating that we are operating in the highly superluminal regime.

Measuring v_i requires an understanding of the fundamental mechanism for information encoding and detection. Garrison *et al.*² propose that new information is encoded on an optical pulse by creating a point that is non-analytic (for example, a discontinuity in the pulse amplitude or its derivatives) and that this point always travels at c regardless of the value of the other velocities associated with the pulse^{2,5}. Essentially, they have generalized Sommerfeld's concept of the front velocity to a non-analytic point of the pulse amplitude, where the front of a square-

shaped pulse is an example of a point of non-analyticity. These workers^{2,5} suggest that the point of non-analyticity is the only part of the pulse representing new information because measurements of the early part of the pulse cannot be used to predict anything about the part of the pulse arriving after the point of non-analyticity, and hence v_i equals the speed of a point of non-analyticity. For counter-views, see refs 2, 4, 23 and 24. We note that some aspects of their proposal have been verified using electronic circuits where no propagating waves are involved, and hence only issues of causality, but not relativistic causality, can be tested^{25–27}.

To enhance our ability to estimate the location of this non-analytic point in the presence of noise, we use two optical pulses that are initially identically gaussian-shaped, which allows us smoothly to turn on the pulse amplitude to a level above the noise floor of our detection electronics and to monitor the fast-light pulse advancement. Near the peak of the gaussian function and at the same moment for both symbols, we switch the amplitude of the gaussian function to a high (1) or low (0) value for the remainder of the pulse. The moment when a decision is made to switch between the symbols corresponds to the point of non-analyticity. Note that this transition is smoothed out by the finite response time of the optical switch.

The location of the point of non-analyticity is determined by detecting the arrival of new information using a receiver that can distinguish between symbols to a desired level of certainty, characterized by the bit error rate (BER). Before the arrival of the point of non-analyticity at the detector, we expect no detected information, corresponding to a BER of 1/2. Once the point of non-analyticity propagates past the detector, the received information will grow smoothly from zero and the BER drops. A symbol is considered to be detected when the BER falls below some threshold. Hence, the detection time of information is later than the time when information is first available at the detector, even for pulses propagating through vacuum. This detection latency Δt depends on the charac-

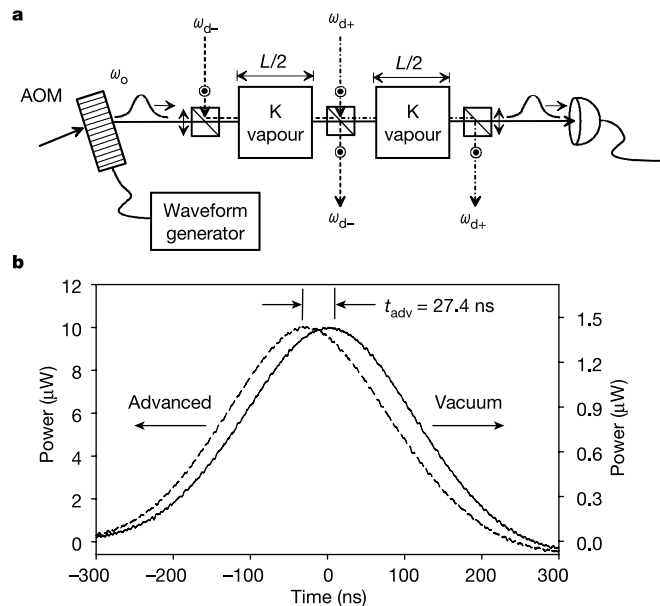


Figure 1 Fast-light pulse propagation. **a**, Experimental set-up. The potassium vapours are contained in two uncoated Pyrex cells of length $L/2 = 20 \text{ cm}$ (to suppress unwanted parametric instabilities²²) and heated to obtain an atomic number density of $4.5 \times 10^{11} \text{ atoms cm}^{-3}$. Linearly polarized coherence-preparation laser beams (frequencies ω_{d-} and ω_{d+}) are combined with the linear and orthogonally polarized pulses using polarizing beam splitters. The pulses are detected by a photoreceiver with a 25 kHz–125 MHz bandwidth. The coherence preparation beams are adjusted with ω_{d-} set at 1.36 GHz to the high-frequency side of the centre of the potassium $4S_{1/2} \leftrightarrow 4P_{1/2}$ transition and $\omega_{d+} - \omega_{d-} = 23 \text{ MHz}$, chosen to optimize the pulse advancement using procedures similar to those discussed in refs 15, 18 and 22. The pulses are generated by passing a continuous-wave laser beam through an acousto-optic modulator (AOM) driven by a computer-controlled arbitrary waveform generator. The time origin has been set arbitrarily to coincide with the peak of this pulse. **b**, The solid line shows the temporal evolution of a 263.4-ns-long (full-width at half-maximum) pulse propagating through the cells when the lasers are tuned far from the atomic resonance and hence the vapour-cell portion of the path is equivalent to vacuum. The dashed line shows the observed fast-light pulse advancement for a smooth pulse shape when the coherence-preparation laser is tuned near the atomic resonance and ω_o is set between the gain resonances. The peak of the pulse is advanced by $t_{\text{adv}} = 27.4 \text{ ns} \pm 1.1 \text{ ns}$, corresponding to a relative pulse advancement of 10.4%. Using $t_{\text{adv}} = L/c - L/v_g$ with $L/c = 1.3 \text{ ns}$, we find $v_g/c = -0.051 \pm 0.002$. Careful inspection of the fast-light pulse reveals that it has been compressed by 1.9%, which is due primarily to the frequency dependence of the gain^{18,19}.

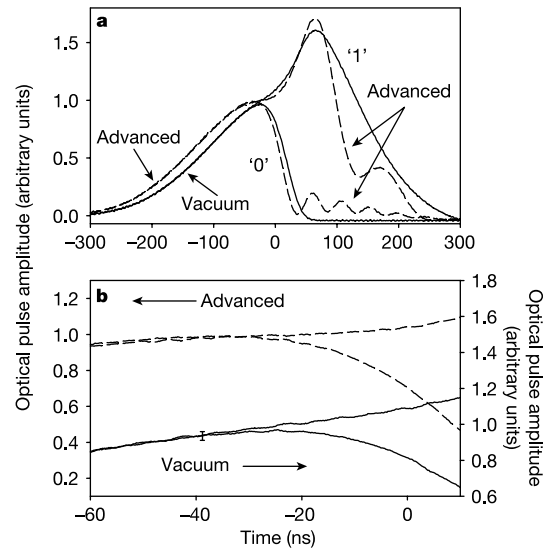


Figure 2 Transmitting information-encoded optical pulses through a fast-light medium. **a**, Transmitting '0' and '1' through the fast-light medium (dashed line) and vacuum (solid line). Each symbol is transmitted separately through the medium and vacuum, where each curve is an average of 50 pulses. **b**, High-resolution plot of part of **a** with an offset for clarity. The amplitude of the advanced and vacuum pulses have been scaled so that their heights would be the same if a gaussian pulse propagated through the system, as in Fig. 1b. The error bar indicates the typical standard deviation of the pulse amplitudes. From **a**, it is seen that the fast-light medium advances the early part of the pulses during the smooth turn on, identically to that observed for the full gaussian-shaped pulses shown in Fig. 1b. Most important is the observation that both symbols are the same for early times so that it is not possible to distinguish between them. Hence, no information can yet be conveyed to a receiving party at the end of the communication channel.

teristics of the medium through which the pulses propagate, the shape of the symbols, the detection algorithm, noise²⁴ in the detection process (including quantum noise^{28,29}), and the BER threshold. It increases as the signal-to-noise ratio decreases because it takes longer for the receiver to achieve the same BER. Achieving the limit $\Delta t \rightarrow 0$ requires the use of optimal symbol shapes and detection algorithms, and infinite energy in the optical pulse so that the signal-to-noise ratio of the detected waveform approaches infinity. Although it is possible to estimate Δt for a specific experimental apparatus, it cannot be measured directly because it requires measuring the point of non-analyticity. A crucial aspect of our experiment is to make Δt as small as possible and to make it as similar as possible for both vacuum and advanced pulses.

Figure 2 shows the propagation of both symbols through the fast-light medium and vacuum. From a simple visual inspection of the data, we see that the time where it is possible to first distinguish between the two symbols for the advanced pulses is slightly later than the time where it is possible to first distinguish between the same two symbols propagating through vacuum. In addition, it is seen that the manner in which the average symbol waveforms separate for the vacuum and advanced case are only slightly different, so that the detection latency times (denoted by Δt_{vac} and Δt_{adv} respectively) should be similar.

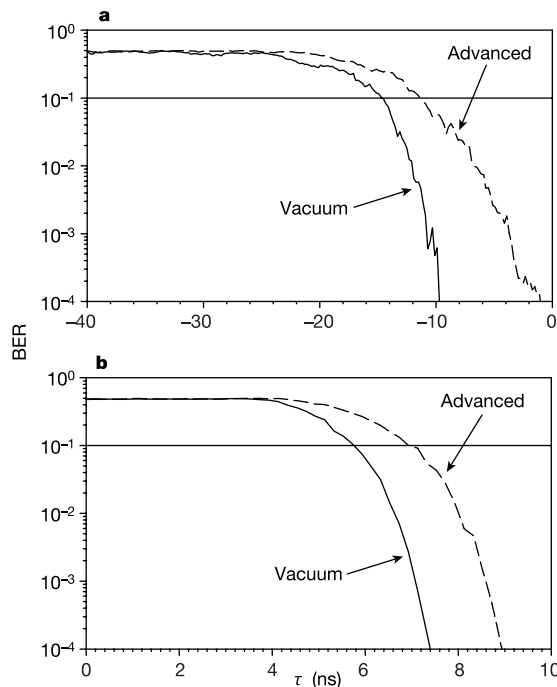


Figure 3 Detecting the arrival of new information. Shown is the BER as a function of the upper limit of the integration time τ for the vacuum (solid line) and advanced (dashed line) pulses. The horizontal line indicates the detection threshold. **a**, Experimental observations. The time origin has been selected arbitrarily. **b**, Theoretical predictions based on Maxwell's equations. The time origin corresponds to the moment when the point of non-analyticity first arrives at the detector. The BER is determined using the following matched-filter procedure. For each symbol (0 and 1), there are 50 pulse waveforms. Reference waveforms, denoted by $R_0(t)$ and $R_1(t)$, are generated by averaging 49 pulse waveforms and the integral $D(\tau) = I_0(\tau) - I_1(\tau)$ is determined for each pulse, where the waveform being detected is not included in the respective reference waveform. Here: $I_j(\tau) = \int_{t_s}^{t_s+\tau} x(t)R_j(t)dt/\alpha_j(\tau_\alpha)N_j(\tau)$ (for $j = 0, 1$), where $x(t)$ is an individual pulse waveform, t_s is an integration start time chosen arbitrarily at a time in the early beginning of the pulse, $N_j(\tau) = \int_{t_s}^{t_s+\tau} R_j^2(t)dt$, $\alpha_j(\tau_\alpha) = \int_{t_s}^{t_s+\tau_\alpha} x^2(t)dt/N_j(\tau_\alpha)$, and τ_α is a normalization integration time chosen arbitrarily on the leading edge of the gaussian pulse before the point where the symbols separate. For each symbol type, the probability density of D is fitted to a gaussian distribution normalized to an area of 1/2 and the overlapping area of these two gaussian distributions is the BER.

To quantify our results, we determine the BER for the vacuum (Fig. 3a, solid line) and advanced (dashed line) pulse pairs using an integrate-and-dump matched filter technique. The BER is high for final observation times in the range between -40 and -25 ns, during which the pulse amplitudes are large (see Fig. 2a). Hence, even though the signal-to-noise ratio for a single pulse is high at these times, the pulses are not yet distinguishable and no information is detected. Placing the detection threshold at $\text{BER} = 0.1$, chosen to keep Δt_{vac} and Δt_{adv} small, we determine the detection time for vacuum (advanced) pulse pairs T_{vac} (T_{adv}) and the difference in detection times $T_i = T_{\text{adv}} - T_{\text{vac}}$. The time difference is approximately constant for BER values around 0.1; its average value in the range of BERs between 0.08 and 0.2 is equal to 3.2 ± 1.5 ns. Our observations demonstrate that the information detection time for pulses propagating through the fast-light medium is longer than the detection time for the same information propagating through vacuum, even though the group velocity is in the highly superluminal regime for the fast-light medium.

From our direct measurement of T_i , we do not know whether an observed difference between the detection times is due to changes in the detection latencies or differences in the information velocities for vacuum ($v_{i,\text{vac}}$) and the fast-light medium ($v_{i,\text{adv}}$). The relation among these quantities is given by:

$$T_i = (L/v_{i,\text{adv}} - L/v_{i,\text{vac}}) + (\Delta t_{\text{adv}} - \Delta t_{\text{vac}}) \quad (1)$$

To gain some insight about the importance of detection latency, we analyse a mathematical model, based on Maxwell's equations, that describes approximately the generation, propagation, and detection of our symbols. Consistent with previous research^{2,5}, this model predicts that $v_{i,\text{adv}} = v_{i,\text{vac}} = c$, and hence T_i is completely determined by $(\Delta t_{\text{adv}} - \Delta t_{\text{vac}})$. Using the same matched-filtering approach, we determine the predicted BER as shown in Fig. 3b. We see that information is detected later for the advanced pulses than for the vacuum pulses, qualitatively similar to the experimental observations. We find that $T_i = 1.5 \pm 0.5$ ns, where the error only accounts for statistical uncertainty in the BER determination. The fact that $T_i \neq 0$ demonstrates that subtle changes in the shape of the symbols after information has been encoded give rise to substantial changes in the detection latency. The predicted value of T_i might be smaller than the observed time owing to our assumption that the fast-light medium does not change the noise properties of the optical pulses²⁸.

Using the model prediction for $(\Delta t_{\text{adv}} - \Delta t_{\text{vac}})$ in equation (1) and taking $v_{i,\text{vac}} = c$, we find that $v_{i,\text{adv}} = 0.4(+0.7 - 0.2)c$. Thus, our observations are consistent with the special theory of relativity even for a medium where v_g is highly superluminal, demonstrating that the peak of the advanced pulse at the exit face of the medium (see Fig. 1b) is not causally connected to the peak at the entrance face². Because our analysis makes no assumptions about the sources of noise in the encoding, transmission and decoding process, our general experimental approach and conclusions should hold even in the limit where quantum fluctuations are dominant^{3,28,29}. \square

Received 11 July; accepted 20 August 2003; doi:10.1038/nature02016.

1. Jackson, J. D. *Classical Electrodynamics* 3rd edn, Sec. 11.3.C (John Wiley & Sons, New York, 1999).
2. Garrison, J. C., Mitchell, M. W., Chiao, R. Y. & Bolda, E. L. Superluminal signals: causal loop paradoxes revisited. *Phys. Lett. A* **245**, 19–25 (1998).
3. Boyd, R. W. & Gauthier, D. J. in *Progress in Optics* (ed. Wolf, E.) Vol. 43, 497–530, Ch. 6 (Elsevier, Amsterdam, 2002).
4. Nimtz, G. & Gaebel, A. Basics of superluminal signals. *Ann. Phys.* **11**, 163–171 (2002).
5. Chiao, R. Y. & Steinberg, A. M. in *Progress in Optics* (ed. Wolf, E.) Vol. 37, 345–405, Ch. 6 (Elsevier Science, Amsterdam, 1997).
6. Agrawal, G. P. *Nonlinear Fiber Optics* 3rd edn, Ch. 1 (Academic, San Diego, 2001).
7. Born, M. & Wolf, E. *Principles of Optics* 7th edn, Sec. 2.3.4 (Cambridge Univ. Press, Cambridge, 1999).
8. Garrett, C. G. B. & McCumber, D. E. Propagation of a Gaussian light pulse through an anomalous dispersion medium. *Phys. Rev. A* **1**, 305–313 (1970).
9. Brillouin, L. *Wave Propagation and Group Velocity* Ch. I (Academic, New York, 1960).
10. Sommerfeld, A. Über die fortpflanzung des liches in dispergierenden medien. *Ann. Phys.* **44**, 177–202 (1914); English translation available in Brillouin, L. *Wave Propagation and Group Velocity* Ch. II (Academic, New York, 1960).
11. Brillouin, L. Über die fortpflanzung des liches in dispergierenden medien. *Ann. Phys.* **44**, 203–240

- (1914); English translation available in Brillouin, L. *Wave Propagation and Group Velocity* Ch. III (Academic, New York, 1960).
12. Chu, C. & Wong, S. Linear pulse propagation in an absorbing medium. *Phys. Rev. Lett.* **48**, 738–741 (1982).
 13. Ségard, B. & Macke, B. Observation of negative velocity pulse propagation. *Phys. Lett.* **109**, 213–216 (1985).
 14. Peatross, J., Glasgow, S. A. & Ware, M. Average energy flow of optical pulses in dispersive media. *Phys. Rev. Lett.* **84**, 2370–2373 (2000).
 15. Wang, L. J., Kuzmich, A. & Dogariu, A. Gain-assisted superluminal light propagation. *Nature* **406**, 277–279 (2000).
 16. Akulshin, A. M., Cimmino, A. & Opat, G. I. Negative group velocity of a light pulse in cesium vapor. *Quantum Electron.* **32**, 567–569 (2002).
 17. Bigelow, M. S., Lepeshkin, N. N. & Boyd, R. W. Superluminal and slow light propagation in a room-temperature solid. *Science* **301**, 200–202 (2003).
 18. Cao, H., Dogariu, A. & Wang, L. J. Negative group delay and pulse compression in superluminal pulse propagation. *IEEE J. Sel. Top. Quantum Electron.* **9**, 52–58 (2003).
 19. Macke, B. & Ségard, B. Propagation of light-pulses at a negative group velocity. *Eur. Phys. J. D* **23**, 125–141 (2003).
 20. Steinberg, A. M. & Chiao, R. Y. Dispersionless, highly superluminal propagation in a medium with a gain doublet. *Phys. Rev. A* **49**, 2071–2075 (1994).
 21. Harris, S. E. Electromagnetically induced transparency. *Phys. Today* **50**, 36–42 (1997).
 22. Stenner, M. D. & Gauthier, D. J. Pump-beam-instability limits to Raman-gain-doublet “fast-light” pulse propagation. *Phys. Rev. A* **67**, 063801 (2003).
 23. Diener, G. Superluminal group velocities and information transfer. *Phys. Lett. A* **223**, 327–331 (1996).
 24. Wynne, K. Causality and the nature of information. *Opt. Commun.* **209**, 85–100 (2002).
 25. Mitchell, M. W. & Chiao, R. Y. Negative group delay and “fronts” in a causal system: An experiment with very low frequency bandpass filters. *Phys. Lett. A* **230**, 133–138 (1999).
 26. Nakanishi, T., Sugiyama, K. & Kitano, K. Demonstration of negative group delays in a simple electronic circuit. *Am. J. Phys.* **70**, 1117–1121 (2002).
 27. Solli, D., Chiao, R. Y. & Hickmann, J. M. Superluminal effects and negative group delays in electronics, and their applications. *Phys. Rev. E* **66**, 056601 (2002).
 28. Kuzmich, A., Dogariu, A., Wang, L. J., Milonni, P. W. & Chiao, R. Y. Signal velocity, causality, and quantum noise in superluminal light pulse propagation. *Phys. Rev. Lett.* **86**, 3925–3929 (2001).
 29. Caves, C. M. & Drummond, P. Quantum limits on bosonic communication rates. *Rev. Mod. Phys.* **66**, 481–537 (1994).

Acknowledgements M.D.S. and D.J.G. acknowledge discussions with M. Gehm and J. Thomas, the loan of an argon-ion pump laser from J. Thomas, and the financial support of the US National Science Foundation.

Competing interests statement The authors declare that they have no competing financial interests.

Correspondence and requests for materials should be addressed to D.J.G. (gauthier@phy.duke.edu).

Single-electron transistor of a single organic molecule with access to several redox states

Sergey Kubatkin¹, Andrey Danilov¹, Mattias Hjort², Jérôme Cornil^{2,3}, Jean-Luc Brédas^{2,3*}, Nicolai Stühr-Hansen⁴, Per Hedegård⁴ & Thomas Bjørnholm⁴

¹Department of Microtechnology and Nanoscience/MC2, University of Technology, Chalmers, Göteborg, Sweden

²Department of Chemistry, The University of Arizona, Tucson, Arizona 85721-0041, USA

³Laboratory for Chemistry of Novel Materials, Center for Research in Molecular Electronics and Photonics, University of Mons-Hainaut, Place du Parc 20, B-7000 Mons, Belgium

⁴Nano-Science Center (Department of Chemistry and Niels Bohr Institute), University of Copenhagen, Universitetsparken 5, DK-2100, Copenhagen, Denmark

* Present address: School of Chemistry and Biochemistry, Georgia Institute of Technology, Atlanta, Georgia 30332-040, USA

A combination of classical Coulomb charging, electronic level spacings, spin, and vibrational modes determines the single-electron transfer reactions through nanoscale systems connected to external electrodes by tunnelling barriers¹. Coulomb charging effects have been shown to dominate such transport in semi-

conductor quantum dots², metallic³ and semiconducting⁴ nanoparticles, carbon nanotubes^{5,6}, and single molecules^{7–9}. Recently, transport has been shown to be also influenced by spin—through the Kondo effect—for both nanotubes¹⁰ and single molecules^{8,9}, as well as by vibrational fine structure^{7,11}. Here we describe a single-electron transistor where the electronic levels of a single π -conjugated molecule in several distinct charged states control the transport properties. The molecular electronic levels extracted from the single-electron-transistor measurements are strongly perturbed compared to those of the molecule in solution, leading to a very significant reduction of the gap between the highest occupied molecular orbital and the lowest unoccupied molecular orbital. We suggest, and verify by simple model calculations, that this surprising effect could be caused by image charges generated in the source and drain electrodes resulting in a strong localization of the charges on the molecule.

We measured electrical transport at 4 K through a single *p*-phenylenevinylene oligomer, which has five benzene rings connected through four double bonds (OPV5, Fig. 1a). OPV5 was placed by chemical vapour deposition in a gap about 2 nm wide separating the source and drain electrodes of a single-electron transistor (SET) device (Fig. 1). The synthesis of OPV5 ((*E,E*)-1,4-bis{4-[(*E*)-4-(*tert*-butylthio)styryl]}benzene) was done by a Horner–Wadsworth–Emmons condensation¹² of tetraethyl 1,4-xylylenediphosphonate with *trans*-4-(*tert*-butylthio)styrylbenzaldehyde. The terminal thiols were protected with a *tert*-butyl group, which prevents chemical binding of the sulphur to the gold electrode and leads to a weak van der Waals contact between the molecule and the source and drain electrodes.

A planar gate electrode made of aluminium metal covered with aluminium oxide (~5 nm thick) was prepared on a chip of oxidized silicon. A shadow mask used to deposit the gold lead electrodes was defined on top of the gate by standard electron-beam lithography. The chip was then introduced into a vacuum chamber immersed in liquid helium. All subsequent procedures reported here were performed during a single vacuum cycle. First, two gold electrodes were deposited through a shadow mask by condensing gold vapour on the substrate held at 4.2 K. By using an oblique evaporation angle (Fig. 1b) together with *in situ* conductance measurements, we were able to fine-tune the tunnelling gap between the gold electrodes to a few nanometres¹³. As shown in Fig. 1b, for an inclined beam, a constriction is formed by two mask edges. If the tilt angle is high, there is no overlap between source and drain shadows. Reducing the tilt angle decreases the source–drain gap. We changed the tilt stepwise, narrowing the gap between the leads by 5 nm at each step. At each step, a 2-nm-thick film of gold was deposited through the mask and the sample was checked for non-zero tunnelling conductance (this procedure of nanometre-scale gap fabrication has been successfully tested for other metals¹³). Eventually, we fabricated two self-aligned and self-sharpened gold electrodes with a tunnelling gap of a few M Ω between them. By annealing the sample up to 100 K, we increased the gap resistance to a few G Ω , which corresponds to a tunnelling gap width of roughly 2 nm (ref. 14). Annealed samples did not show any gate dependence of the tunnelling conductance nor any peculiarities in the current–voltage, *I*(*V*), curves. In a separate control experiment, we observed that an irreversible decomposition of gold into separate clusters starts at 150–200 K.

Second, a submonolayer (~1%) of organic molecules was deposited on the electrodes by quench condensation. The sample was annealed at low temperature (below 70 K) allowing thermally activated motion of the organic molecules, while monitoring the nanogap conductance at a source–drain bias of 400 mV. When the conductance changed stepwise, indicating the trapping of a single molecule in the nanogap, the device was cooled to a temperature of 4.2 K where all transport measurements were taken. This entire process was repeated successfully for three independent devices.